

Title: Brain Morphology Normative modelling platform for abnormality and Centile estimation: *Brain MoNoCle*

Authors: Bethany Little^{1,2}, Nida Alyas¹, Alexander Surtees³,
Gavin P Winston^{4,5}, John S Duncan⁴, David A Cousins^{2,6}, John-Paul Taylor²,
Peter Taylor^{1,2,4}, Karoline Leiberg^{1‡}, Yujiang Wang^{1,2,4*‡}

June 28, 2024

Affiliations:

1. CNNP Lab (www.cnnp-lab.com), School of Computing, Newcastle University; Newcastle upon Tyne, United Kingdom.
2. Faculty of Medical Sciences, Newcastle University; Newcastle upon Tyne, United Kingdom.
3. Research Software Engineers, Newcastle University; Newcastle-upon-Tyne, United Kingdom.
4. UCL Queen Square Institute of Neurology; Queen Square, London, United Kingdom.
5. Department of Medicine (Division of Neurology), Queen's University; Kingston, Canada.
6. Cumbria, Northumberland Tyne and Wear NHS Foundation Trust; Newcastle upon Tyne, United Kingdom.

* Yujiang.Wang@newcastle.ac.uk

‡ Joint senior authors

Abstract:

Normative models of brain structure estimate the effects of covariates such as age and sex using large samples of healthy controls. These models can then be applied to smaller clinical cohorts to distinguish disease effects from other covariates. However, these advanced statistical modelling approaches can be difficult to access, and processing large healthy cohorts is computationally demanding. Thus, accessible platforms with pre-trained normative models are needed.

We present such a platform for brain morphology analysis as an open-source web application <https://cnnplab.shinyapps.io/normativemodelshiny/>, with six key features: (i) user-friendly web interface, (ii) individual and group outputs, (iii) multi-site analysis, (iv) regional and whole-brain analysis, (v) integration with existing tools, and (vi) featuring multiple morphology metrics.

Using a diverse sample of 3,276 healthy controls across 21 sites, we pre-trained normative models on various metrics. We validated the models with a small clinical sample of individuals with bipolar disorder, showing outputs that aligned closely with existing literature only after applying our normative modelling. Further validation with a cohort of temporal lobe epilepsy showed agreement with previous group-level findings and individual-level seizure lateralisation. Finally, with the ability to investigate multiple morphology measures in the same framework, we found that biological covariates are better explained in specific morphology measures, and for clinical applications, only some measures are sensitive to the disease process.

Our platform offers a comprehensive framework to analyse brain morphology in clinical and research settings. Validations confirm the superiority of normative models and the advantage of investigating a range of brain morphology metrics together.

1 Introduction

Brain morphology, the study of the shape and size of brain structures, can be used to track healthy brain development and detect abnormalities associated with underlying disease processes. Normative modelling of brain morphology uses large and diverse datasets to estimate healthy variance across the lifespan. In clinical research, normative models can reliably remove biological and technical covariates from unseen data without removing disease effects (1), which is especially valuable for small samples with a limited number of control subjects. Further, the ability of normative modelling to estimate abnormalities in individuals is crucial for clinical applications, as it enables systematic biomarker discovery and supports translational uses in diagnosis, stratification, and localisation (2–4). Therefore, normative modelling of brain morphology is an indispensable framework that should be available and accessible to all researchers.

To enable researchers without high levels of technical/statistical know-how to benefit from the power of the normative modelling framework, a freely-available, pre-trained modelling platform is needed. The normative models should be based on large, diverse, healthy population data, and be easily-applied to new data. Recent efforts in this field include several open-source tools, some allowing users to upload new, unseen brain morphology data to a web interface and generate individual abnormality scores (e.g. z-scores or centiles) (5–7). Each of these tools have some advantages: for example, (i) being accessible as an online tool that can be easily-used without any need for software download/installation or writing/running scripts, (ii) providing individual and group-level outputs, (iii) multi-site data - as often seen in clinical research - can be analysed, (iv) analysing brain shape on whole hemispheres and smaller regions, (v) seamless integration with existing neuroimaging software such as FreeSurfer, and (vi) the option to explore a variety of metrics.

We present a normative modelling tool of brain morphology that combines all six key features in one open and web-based application: Brain MoNoCle (Brain Morphology Normative modelling platform for abnormality and Centile estimation). We included a large and diverse sample of 3,276 healthy controls across 21 sites to pre-train normative models in a variety of brain morphology measures that comprehensively quantify cortical shape, including three novel metrics that were only

recently proposed (8). As a first validation, we demonstrate how normative modelling improves reliability and reproducibility in a small clinical dataset of individuals with bipolar disorder (BD). We further validate our outputs in a dataset of temporal lobe epilepsy (TLE) at the group-level, and illustrate how individual patient abnormality scores agree with their seizure lateralisation. Finally, with the option to explore a variety of morphology metrics on our platform, we highlight the importance of investigating multiple metrics at the same time both for normative modelling itself, but also for clinical applications.

2 Results

2.1 Pre-trained normative models on web platform

To pre-train normative models, we used data from 3,276 healthy individuals from several large public and in-house datasets, detailed in Supplementary S1 (9–18). We focused on including a variety of scanning protocols/sites (total 21 sites) to enable mixed-effect modelling, and we achieved a larger overall sample size than recommended by previous normative models (7). The age in the total normative dataset ranged from 5 to 95 years old and is shown by data source in Fig. 1. With this data we pre-trained our normative models for the whole hemisphere, each brain region, and morphology metric (see Methods for details of statistical models). We incorporated these pre-trained normative models on a web platform (Brain MoNoCle) to allow users to upload their own datasets to find morphological abnormalities in individuals and groups. In the following, we will validate our normative modelling framework and web platform outputs in a variety of ways, and demonstrate some biological insight.

2.2 Cortical thickness abnormalities in a bipolar sample more closely match previous findings when using the normative model

To validate the normative modelling framework and outputs, we first investigated the group-level differences in a small, well-defined clinical cohort of bipolar disorder (BD, n=56) and matched controls (BD-HC, n=26). We specifically wanted to see the difference in outputs between using

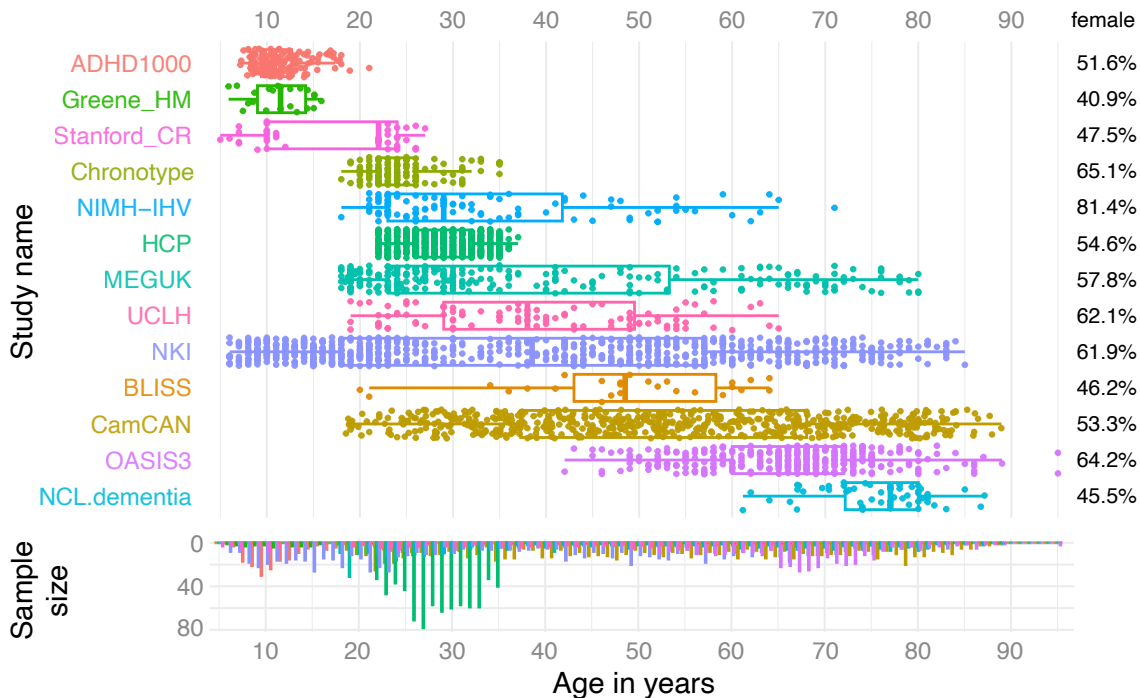


Fig. 1: Demographics of the data underlying the normative model. Age distributions and proportion of female participants are shown for each study.

a traditional case-control comparison approach only using the matched controls (Figure 2 A) *vs.* using our normative model instead (Figure 2 B). When using the small BD-HC group, effect sizes (Cohen’s d) suggested that cortical thinning was greatest in the left post-central gyrus ($d=-0.85$) and that the cortex was thicker in BD in the left pre-central gyrus ($d=0.70$). However, when using the normative model pipeline, the same sample showed similar thinning in the left post-central gyrus ($d=-0.83$), but cortical *thinning* in the left pre-central gyrus ($d=-0.8$). The latter of these findings, obtained through normative modelling, is more in line with previous findings from a large sample ENIGMA study (19).

2.3 Group-level cortical thickness abnormalities in mesial temporal lobe epilepsy agree with previous findings

We validated our normative model outputs in a large sample of individuals with mTLE (74 left mTLE, 59 right mTLE) and matched controls ($n=99$) (20). Figure 3 shows cortical thickness abnormality estimates for right mTLE and left mTLE groups. We found widespread cortical

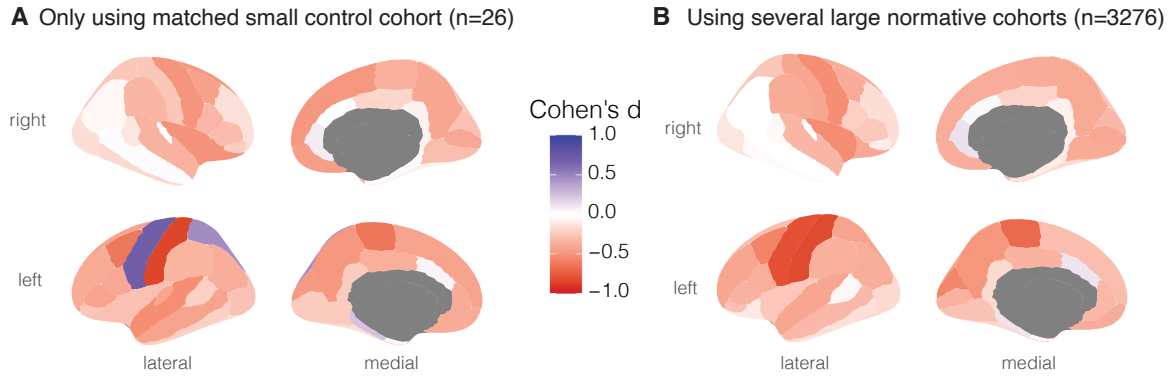


Fig. 2: Alterations in cortical thickness associated with bipolar disorder derived from a case-control study *vs.* normative modelling. Group-level abnormalities in cortical thickness in $n=56$ people with bipolar disorder for: **A** a small, matched control group ($n=26$); and **B** the normative reference population ($n=3,276$).

thinning, especially in the right mTLE group, in cortical regions including the precentral gyrus, supramarginal gyrus, and inferior parietal gyrus. This result reproduces both the findings from the IDEAS and ENIGMA-epilepsy studies (20, 21).

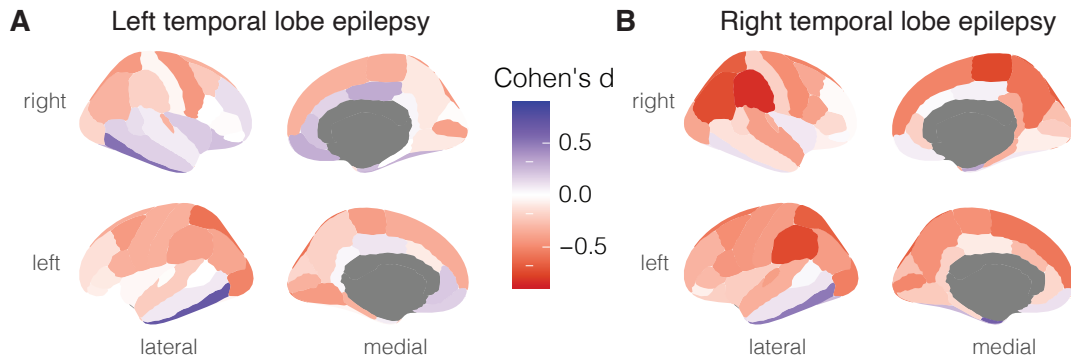


Fig. 3: Group-level output for mesial temporal lobe epilepsy cohort after normative modelling. Group-level summary of abnormalities in cortical thickness for left mTLE ($n=74$, **A**) and right mTLE ($n=59$, **B**), showing Cohen's d effect size for each cortical region.

2.4 Individual-level abnormalities in certain measures agree with clinical lateralisation of seizure onset

To validate individual-level outputs and abnormalities, we used seizure lateralisation from the IDEAS dataset (20). For each subject, we extracted the z-score difference between left and right hemisphere in cortical thickness and other metrics (Figure 4). Controls, as expected, had a distri-

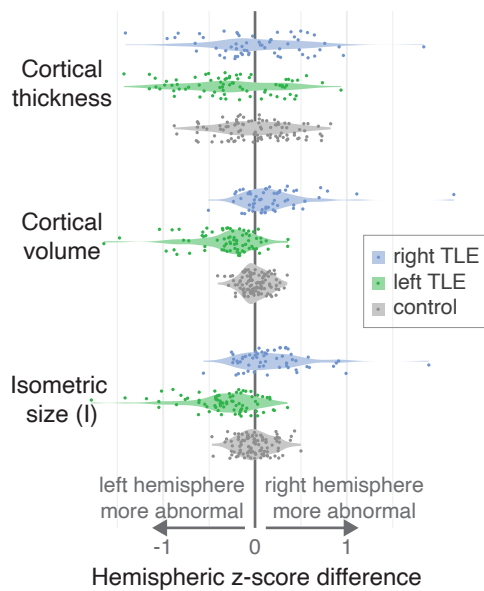


Fig. 4: Individual-level z-scores after normative modelling for mTLE cohort. Difference in hemisphere-level z-score between left and right hemisphere is shown in controls and right/left TLE subgroups for three example morphological measures. Individual subjects are shown as single data points, distributions of subjects are displayed as violin plots.

bution around zero in all measures after regressing out healthy biological covariates.

The measure most frequently-used in cortical morphometry, cortical thickness, did not lateralise individual patients well, and most patient z-scores differences were within the same range and distribution as the controls.

Given that our normative modelling platform offers the ability to analyse multiple morphology measures, and given that cortical thickness is known to covary with other measures (such as surface area and volume), we investigated all metrics implemented on the platform. This included three statistically independent novel measures. We demonstrated that both cortical volume and I - our novel morphometric for isometric size - were best at lateralising at the hemisphere level (Figure 4). Specifically, for cortical volume, most (78.2%) patients had a z-score difference greater/smaller than zero indicating lateralisation in agreement with clinical metadata. For I, 75.9% of patients showed the correct laterality. Further, 36.1% of patients were outside of 2 standard deviations of the control for cortical volume, and 32.3% for I.

2.5 Covariates explain more variance in independent component K than in other structural MRI measures

Given the observed specificity in particular measures for seizure lateralisation, we explored the differences between morphological measures further to establish a baseline for future applications. To this end, we investigated the normative models accounting for age, sex and scanning site for each measure.

Figure 5 A and B show the fitted normative model over age for two example measures: cortical thickness and K - a novel independent morphometric that is known to change with age (8). Both thickness and K decrease over age with steeper declines in early and later life.

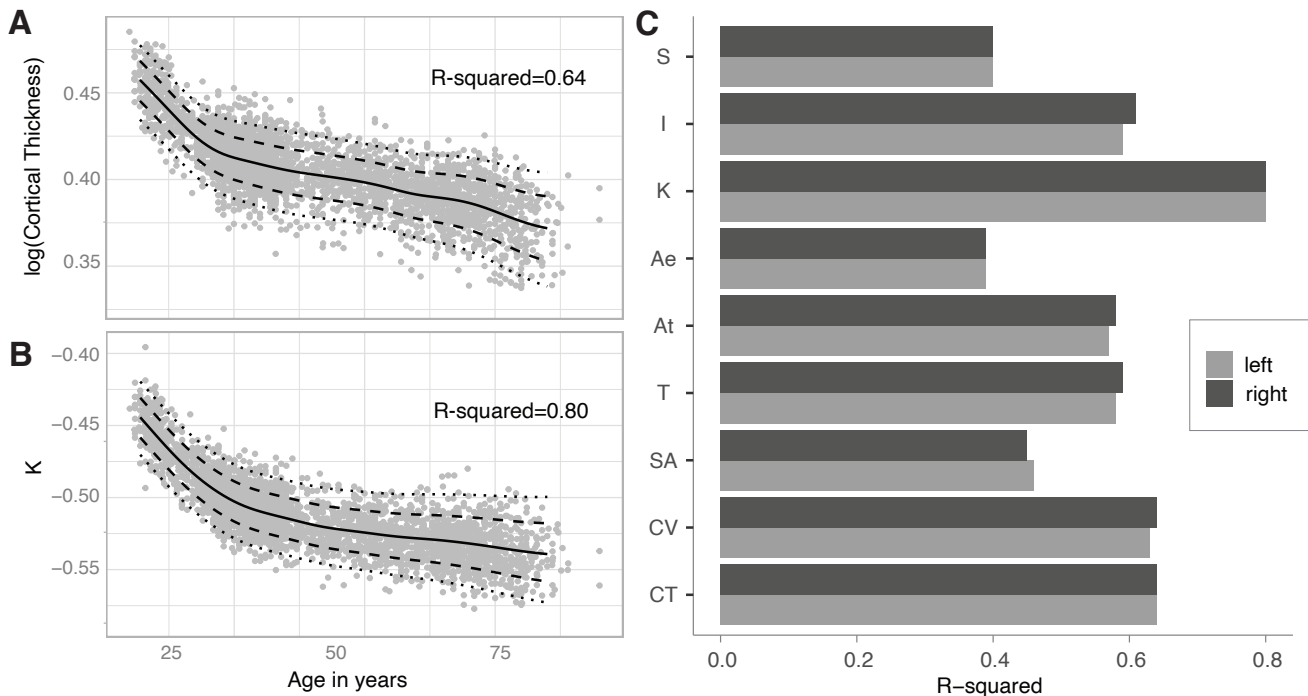


Fig. 5: Variance explained by normative model in each morphometric. A & B Harmonised normative data (grey dots) and predicted model centiles of mean cortical thickness and K across the lifespan (n=3,276). C Model fit statistics R^2 for each metric and hemisphere. CT, CV, and SA are structural metrics estimated using FreeSurfer; T, At, Ae, K, I and S are structural metrics estimated using the Cortical Folding toolbox. CT=cortical thickness, CV=cortical volume, SA=surface area; T=average thickness, At=total pial surface area, Ae=exposed surface area.

To compare morphology measures more directly, we obtained the R^2 of the normative model fit for each measure Figure 5 C. All measures used the same statistical model formulas of age, sex and site. Out of all the measures implemented, K shows the best model fit ($R^2 = 0.8$ for both left

and right hemisphere), superior to all other metrics with R^2 around or below 0.6.

3 Discussion

Summary: Brain MoNoCle is a user-friendly online normative modelling platform for brain morphology analysis. The platform combines and unifies the most frequently-requested and desired features of existing approaches and toolboxes in one, importantly including the option to analyse multiple morphology measures under one framework. We validated our normative models and platform outputs in clinical cohorts through a series of tests, including replicating previous findings from ENIGMA studies. We also provided an individual-level output validation in a sample of mTLE by demonstrating agreement of our outputs with the clinical seizure lateralisation. Particularly, we highlighted that both biological covariates, as well as disease processes, are uniquely expressed in different morphological measures. This implies that brain normative modelling should be performed in a range of measures to be useful for brain morphology analysis in health and disease.

Validations: We demonstrated how our pipeline can be applied to clinical datasets and what outputs can be obtained in a sample of people with BD, and a sample of people with mTLE. Compared to the traditional case-control pipeline, in which BD patients were compared to matched healthy controls, our normative pipeline yielded abnormality estimates that were more in line with previous research, for example a large-scale ENIGMA study of cortical thickness in BD, despite a relatively small patient sample (19). In mTLE, we showed results similar to a recent report of the data-release (20). In particular, we did not find large abnormalities in mTLE patients; this may be because we only show cortical data and mTLE is associated with structural changes in subcortical regions, such as the hippocampus (21). We also tested for lateralisation of the hemispheric abnormalities, and found a generally good agreement with clinical metadata, despite only using cortical data. The reported effect sizes compared to controls are in line with previous reports of lateralisation using cortical information only (21, 22). We conclude that our normative models provide reasonable outputs in small and large samples, and that individual-level outputs are also in line with expectations. We hope Brain MoNoCle will be helpful in future analysis of

cortical morphology.

Methodological advance: Our normative models and web platform is an addition to existing free toolboxes for modelling cortical morphometry (5–7). Brain MoNoCle, however, differs to all of these in some ways, including: No requirement for any coding or running scripts from the user; no need to download software; outputs include group-level analysis compared to controls as well as individual abnormalities as z-scores and centiles; analysis is on full hemispheres and regions; and outputs are visualised in plots and available as tables of z-scores and centiles. There are differences in the underlying models as well. For example, our model harmonises scanning site effects for mean and variance, avoiding separate steps as found in Combat (23), which makes separate assumptions; information is pooled from the male and female populations to directly estimate sex covariate effects; and we use flexible smooth terms for age effects and explicitly model skew and kurtosis with GAMLSS. Lastly, our web platform includes normative models of a range of metrics, including traditional measures like thickness, volume, and pial surface area, but also independent morphometrics which account for the covariance of those measures.

New biological insight: Through our exploration of multiple cortical morphometrics, we were able to compare normative models for traditional measures, such as cortical thickness and surface area, but also novel statistically independent morphometrics. We found that one of these novel morphometrics “K” (also termed “tension component”) displayed a far superior performance as a normative model of age and sex with $R^2 = 0.8$ compared to other morphometrics that achieve R^2 between 0.4 and 0.6. This observation has two implications: firstly, there might be better morphometrics to use to model age and sex effects, and extract disease-specific effects, as alluded to in the first paper proposing “K” as a novel morphometric (8). Secondly, traditional morphometrics clearly have residual unexplained variance due to their statistical interdependence. This implies that investigations of measures such as cortical thickness, and surface area should consider their covariance, rather than interpreting them in isolation. The cortex, as a biological structure obeying physical constraints, clearly does not have independent processes to develop its thickness vs. surface area vs. overall size. Our platform, offering analysis streams for all traditional morphometrics and novel morphometrics therefore serves as a starting point for future statistically robust analyses of

brain morphology.

Roadmap for future development: We have three concrete developments planned for our normative modelling platform. First, we will incorporate recently-proposed multiscale morphometrics (24–26) to allow users to access the most recent cutting-edge developments in morphological analysis. Second, we currently use one Freesurfer parcellation of the brain to analyse finer regions. We plan to incorporate more atlases, and in the same step, incorporate the possibility to jointly model related regions (e.g. neighbouring regions) to increase robustness of the model. Third, with the increasing availability of longitudinal data, we plan to extend our normative model to accept multi-session longitudinal clinical datasets and statistically account for these adequately (see e.g. Bučková et al. (27) for some suggestions). Further, we will add more normative data from diverse geographical areas. We will also implement analysis capacity to compare morphology measures more directly on the web platform. Finally, we aim to add more structural metrics such as subcortical volumes.

4 Materials and methods

4.1 Normative data

We collated 3T T1-weighted MRI scans from 3,276 healthy individuals from several large public and in-house datasets, detailed in Supplementary S1 (9–18). The age in the total dataset ranged from 5 to 95 years old; the age range and sex distribution for each study is illustrated in Figure 1. Scanning protocols differed across, and sometimes within, datasets, which we corrected statistically in a later step. All studies had ethical approval from relevant institutional ethics boards and included written consent from participants. We present here the initial dataset included in v1.0 of our app; however, we aim to continuously add to our normative reference dataset. Users of our web platform should therefore check the latest summary of the dataset when reporting their own results.

4.2 Pre-processing

T1-weighted MRI scans were pre-processed in FreeSurfer (28) using the standard *recon-all* pipeline, which includes removal of non-brain tissue, segmentation of grey and white matter surfaces, and cortical parcellation. We also ran the localGI pipeline (29) to yield smoothed outer pial surfaces. The *aparcstats2table* command was used to generate measures of cortical thickness, cortical volume, and pial surface area, for 68 brain regions according to the Desikan-Killiany parcellation atlas (30). The version of FreeSurfer varied across datasets (see Supplementary S1), which was corrected during site harmonisation.

4.3 Cortical morphology measures

The traditional morphological measures of cortical thickness, pial surface area, and exposed surface area are known to covary (31). Failure to account for this covariance can lose and confuse information about the complex, folded shape of the brain. A recently developed framework proposed a universal scaling law of cortical folding that accounts for covariance between cortical thickness, pial surface area, and exposed surface area (32). From this scaling law, three biologically interpretable independent components, K, I, and S can be derived for hemispheres, lobes, and individual regions (8, 31, 33, 34). The dimensionless measure K reflects tension acting on the cortex and is relatively preserved across species, but appears to be sensitive to ageing and disease processes (8, 33, 34). Isometric term I is orthogonal and statistically independent to K and captures information about isometric size. S is a cross-product of K and I that captures all remaining information about shape, reflecting complexity of cortical folding. For example, if a cortical structure is isometrically rescaled in all dimensions, it changes I, but not K or S. K, I, and S are orthogonal and statistically independent to each other.

As an example, in TLE, these components captured structural changes that were not detected with traditional metrics (8). K, I, and S therefore offer a novel re-conceptualisation of brain morphology measures that can detect nuanced morphological abnormalities. We used the toolbox developed by Wang et al. (8) (<https://github.com/cnmp-lab/CorticalFoldingAnalysisTools>) to calculate K, I, and S for each hemisphere.

4.4 Quality control

Some of the public datasets included quality control steps as part of the study design, which are reported in the original study publications. We detected outliers in the entire dataset statistically: we ran our *gamlss* model described below for each structural metric for each region, and flagged outliers defined by residuals more than five median absolute deviations. In addition, we also detected outliers based on visual inspections of plots: for each dataset, we plotted each brain metric at the hemisphere level against age to flag outliers within each dataset. These were then cross-checked with outliers that were detected statistically. We excluded participants who were flagged as an outlier in any of these models; we performed listwise deletion rather than pairwise deletion so that the same normative reference dataset was used for each normative model, allowing comparisons of model statistics across models.

4.5 Exemplar clinical datasets

To demonstrate the utility of our normative models in predicting abnormalities in patient groups and individuals, we included two exemplar clinical datasets. A sample of 133 adults with mesial TLE (mTLE; n=74 right hemisphere seizure onset; n=59 left hemisphere seizure onset) and 99 healthy controls (HC-mTLE) were acquired from the recent IDEAS dataset release (20), which was approved by a Research Ethics Committee (22/SC/0016). We also included a sample of 56 adults with bipolar disorder (BD) and 26 healthy controls (HC-BD) from the Bipolar Lithium Imaging and Spectroscopy Study (BLISS) (4, 35). The study was granted a favourable ethical opinion by a United Kingdom National Research Ethics Committee (14/NE/1135), and all participants provided written informed consent.

Descriptive statistics for these datasets are summarised in Table 1. See the respective publications for full details of each sample and neuroimaging pre-processing steps.

4.6 Normative models

All brain metrics were log-transformed before being passed into the normative models, so different metrics measuring different dimensionalities (e.g. thickness *vs.* surface area) can be treated

	BD	HC-BD	mTLE left	mTLE right	HC-mTLE
n	56	26	74	59	99
Age [mean (SD)]	45.36 (12.15)	48.46 (11.80)	36.0 (11.2)	38.2 (10.8)	39.1 (12.1)
Sex [n female (%)]	35 (62%)	12 (46%)	43 (58%)	39 (66%)	62 (63%)

Table 1: Demographics of two clinical datasets. SD=standard deviation; HC=healthy controls; BD=bipolar disorder; mTLE=mesial temporal lobe epilepsy.

in the same way for the normative model. Generalized additive models for location scale and shape (GAMLSS) using the gamlss package (<https://cran.r-project.org/web/packages/gamlss/>) were used to simultaneously model the parameters (mean, standard deviation, skew, and kurtosis) of the distribution as response variables of the explanatory variables sex, age, and scanning site. Specifically, in our model: the mean depends on sex (fixed effect), site (random effect), and a smooth function of age; the standard deviation depends on sex (fixed effect), site (random effect), and a smooth function of age; the skew depends on sex (fixed effect) and a smooth function of age; and the kurtosis depends on a smooth function of age. See the Supplementary S2 for a more detailed description and justification of the statistical model. Normative models were generated independently for each region (Desikan-Killiany atlas) and hemisphere independently for each morphometric feature. The residuals of each model were retained and normalised (z-scored) to provide indications of abnormalities and centiles were calculated based on predicted mean, variance, skew, and kurtosis.

4.7 Predicting abnormalities in unseen clinical data

Our analysis pipeline uses the normative models to predict abnormality scores for unseen individuals. First, we predicted the distribution parameters for each new individual based on their age and sex and calculated residuals relative to one of the normative scanning sites; the mean of the residuals from the healthy controls (HCs) in the unseen data was then used to calculate the site-specific offset needed to harmonise the unseen dataset with the normative data. We then

calculated the residuals for each individual relative to their site mean and divided by the standard deviation predicted by the normative model. If there were 30 or more HCs in the unseen dataset, we estimated the standard deviation from the unseen HCs, otherwise, we used the mean of the site-specific standard deviation across normative sites. We then used this site-specific standard deviation to z-score the unseen individuals. The site-specific mean and standard deviation, and the skew and kurtosis from the normative model, were used to calculate centiles. See the Supplementary S2 for a detailed description of the statistical pipeline.

4.8 Using Brain MoNoCle

To run our pipeline to predict abnormalities in unseen data as described above, we used our platform Brain MoNoCle. Users can follow the same steps to run the pipeline on their own data. First, we uploaded pre-processed brain imaging data. For traditional brain imaging metrics, data should be pre-processed using FreeSurfer (e.g., the standard *recon-all* command) and the structural metrics for each hemisphere should be exported as csv files using the *aparcstats2table* command; then the csv file for each hemisphere can be directly uploaded to our app. For independent components, the output of our cortical folding toolbox (<https://github.com/cnnp-lab/CorticalFoldingAnalysisTools>) can be directly uploaded. We also uploaded meta-data in a csv file containing subject IDs, age, sex, group, dataset, scanning site, and session. After selecting 'Run Model' to start the analysis, z-scores, group summary statistics, and centiles are available to view and download as csv files, using the tabs in the main panel. Users can export plots by selecting the 'Brain plot' and 'Scatter plot' tabs. A html report is available to download using the 'Report' tab.

4.9 Statistical analysis

All statistical analysis was performed in R Studio v4.3.2. Each test and associated sample size is stated in the results section. Raw p-values are only reported for reference, and not to draw conclusions about significance, or to sub-select samples for downstream analyses.

References and Notes

- [1] Raymond Pomponio, Guray Erus, Mohamad Habes, Jimit Doshi, Dhivya Srinivasan, Elizabeth Mamourian, Vishnu Bashyam, Ilya M. Nasrallah, Theodore D. Satterthwaite, Yong Fan, Lenore J. Launer, Colin L. Masters, Paul Maruff, Chuanjun Zhuo, Henry Völzke, Sterling C. Johnson, Jurgen Fripp, Nikolaos Koutsouleris, Daniel H. Wolf, Raquel Gur, Ruben Gur, John Morris, Marilyn S. Albert, Hans J. Grabe, Susan M. Resnick, R. Nick Bryan, David A. Wolk, Russell T. Shinohara, Haochang Shou, and Christos Davatzikos. Harmonization of large mri datasets for the analysis of brain imaging patterns throughout the lifespan. *NeuroImage*, 208, 2020. ISSN 10959572. doi: 10.1016/j.neuroimage.2019.116450.
- [2] Flavia Loreto, Serena Verdi, Seyed Mostafa Kia, Aleksandar Duvnjak, Haneen Hakeem, Anna Fitzgerald, Neva Patel, Johan Lilja, Zarni Win, Richard Perry, Andre F. Marquand, James H. Cole, and Paresh Malhotra. Alzheimer’s disease heterogeneity revealed by neuroanatomical normative modeling. *Alzheimer’s & Dementia: Diagnosis, Assessment & Disease Monitoring*, 16:e12559, 1 2024. ISSN 2352-8729. doi: 10.1002/DAD2.12559.
- [3] Peter N Taylor, Christoforos A Pappasavvas, Thomas W Owen, Gabrielle M Schroeder, Frances E Hutchings, Fahmida A Chowdhury, Beate Diehl, John S Duncan, Andrew W McEvoy, Anna Miserocchi, Jane de Tisi, Sjoerd B Vos, Matthew C Walker, and Yujiang Wang. Normative brain mapping of interictal intracranial eeg to localize epileptogenic tissue. *Brain*, 145:939–949, 4 2022. ISSN 0006-8950. doi: 10.1093/BRAIN/AWAB380.
- [4] Bethany Little, Carly Flowers, Andrew Blamire, Peter Thelwall, John-Paul Taylor, Peter Gallagher, David Andrew Cousins, and Yujiang Wang. Multivariate brain-cognition associations in euthymic bipolar disorder. *arXiv*, arXiv:2311.01543, 11 2023. doi: 10.48550/arXiv.2311.01543. URL <https://arxiv.org/abs/2311.01543v1>.
- [5] Saige Rutherford, Pieter Barkema, Ivy F Tso, Chandra Sripada, Christian F Beckmann, Henricus G Ruhe, and Andre F Marquand. Evidence for embracing normative modeling. *eLife*, 12:e85082, 2023. doi: 10.7554/eLife.85082.

- [6] R. A. I. Bethlehem, J. Seidlitz, S. R. White, J. W. Vogel, K. M. Anderson, C. Adamson, S. Adler, G. S. Alexopoulos, E. Anagnostou, A. Areces-Gonzalez, D. E. Astle, B. Auyeung, M. Ayub, J. Bae, G. Ball, S. Baron-Cohen, R. Beare, S. A. Bedford, V. Benegal, F. Beyer, J. Blangero, M. Blesa Cábiz, J. P. Boardman, M. Borzage, J. F. Bosch-Bayard, N. Bourke, V. D. Calhoun, M. M. Chakravarty, C. Chen, C. Chertavian, G. Chetelat, Y. S. Chong, J. H. Cole, A. Corvin, M. Costantino, E. Courchesne, F. Crivello, V. L. Croypley, J. Crosbie, N. Crossley, M. Delarue, R. Delorme, S. Desrivieres, G. A. Devenyi, M. A. Di Biase, R. Dolan, K. A. Donald, G. Donohoe, K. Dunlop, A. D. Edwards, J. T. Ellison, C. T. Ellis, J. A. Elman, L. Eyler, D. A. Fair, E. Feczko, P. C. Fletcher, P. Fonagy, C. E. Franz, L. Galan-Garcia, A. Gholipour, J. Giedd, J. H. Gilmore, D. C. Glahn, I. M. Goodyer, P. E. Grant, N. A. Groenewold, F. M. Gunning, R. E. Gur, R. C. Gur, C. F. Hammill, O. Hansson, T. Hedden, A. Heinz, R. N. Henson, K. Heuer, J. Hoare, B. Holla, A. J. Holmes, R. Holt, H. Huang, K. Im, J. Ipser, C. R. Jack Jr, A. P. Jackowski, T. Jia, K. A. Johnson, P. B. Jones, D. T. Jones, R. S. Kahn, H. Karlsson, L. Karlsson, R. Kawashima, E. A. Kelley, S. Kern, K. W. Kim, M. G. Kitzbichler, W. S. Kremen, F. Lalonde, B. Landeau, S. Lee, J. Lerch, J. D. Lewis, J. Li, W. Liao, C. Liston, M. V. Lombardo, J. Lv, C. Lynch, T. T. Mallard, M. Marcelis, R. D. Markello, S. R. Mathias, B. Mazoyer, P. McGuire, M. J. Meaney, A. Mechelli, N. Medic, B. Mistic, S. E. Morgan, D. Mothersill, J. Nigg, M. Q. W. Ong, C. Ortinau, R. Ossenkoppele, M. Ouyang, L. Palaniyappan, L. Paly, P. M. Pan, C. Pantelis, M. M. Park, T. Paus, Z. Pausova, D. Paz-Linares, A. Pichet Binette, K. Pierce, X. Qian, J. Qiu, A. Qiu, A. Raznahan, T. Rittman, A. Rodrigue, C. K. Rollins, R. Romero-Garcia, L. Ronan, M. D. Rosenberg, D. H. Rowitch, G. A. Salum, T. D. Satterthwaite, H. L. Schaare, R. J. Schachar, A. P. Schultz, G. Schumann, M. Schöll, D. Sharp, R. T. Shinohara, I. Skoog, C. D. Smyser, R. A. Sperling, D. J. Stein, A. Stolicyn, J. Suckling, G. Sullivan, Y. Taki, B. Thyreau, R. Toro, N. Traut, K. A. Tsvetanov, N. B. Turk-Browne, J. J. Tuulari, C. Tzourio, É. Vachon-Preseau, M. J. Valdes-Sosa, P. A. Valdes-Sosa, S. L. Valk, T. van Amelsvoort, S. N. Vandekar, L. Vasung, L. W. Victoria, S. Villeneuve, A. Villringer, P. E. Vértes, K. Wagstyl, Y. S. Wang, S. K. Warfield, V. Warriar, E. Westman, M. L. Westwater, H. C. Whalley,

A. V. Witte, N. Yang, B. Yeo, H. Yun, A. Zalesky, H. J. Zar, A. Zettergren, J. H. Zhou, H. Ziauddeen, A. Zugman, X. N. Zuo, 3R-BRAIN, AIBL, Alzheimer’s Disease Neuroimaging Initiative, Alzheimer’s Disease Repository Without Borders Investigators, CALM Team, Cam-CAN, CCNP, COBRE, cVEDA, ENIGMA Developmental Brain Age Working Group, Developing Human Connectome Project, FinnBrain, Harvard Aging Brain Study, IMAGEN, KNE96, The Mayo Clinic Study of Aging, NSPN, POND, The PREVENT-AD Research Group, VETSA, E. T. Bullmore, and A. F. Alexander-Bloch. Brain charts for the human lifespan. *Nature*, 604:525–533, 2021. ISSN 14764687. doi: 10.1038/s41586-022-04554-y.

- [7] Ruiyang Ge, Yuetong Yu, Yi Xuan Qi, Yu nan Fan, Shiyu Chen, Chuntong Gao, Shalaila S Haas, Faye New, Dorret I Boomsma, Henry Brodaty, Rachel M Brouwer, Randy Buckner, Xavier Caseras, Fabrice Crivello, Eveline A Crone, Susanne Erk, Simon E Fisher, Barbara Franke, David C Glahn, Udo Dannlowski, Dominik Grotegerd, Oliver Gruber, Hilleke E Hulshoff Pol, Gunter Schumann, Christian K Tamnes, Henrik Walter, Lara M Wierenga, Neda Jahanshad, Paul M Thompson, Sophia Frango, and ENIGMA Lifespan Working Group. Normative modelling of brain morphometry across the lifespan with centile-brain: algorithm benchmarking and model optimisation. *The Lancet. Digital health*, 6: e211–e221, 3 2024. ISSN 2589-7500. doi: 10.1016/S2589-7500(23)00250-9. URL <http://www.ncbi.nlm.nih.gov/pubmed/38395541>.
- [8] Yujiang Wang, Karoline Leiber, Tobias Ludwig, Bethany Little, Joe H. Nesus, Gavin Winston, Sjoerd B. Vos, Jane de Tisi, John S. Duncan, Peter N. Taylor, and Bruno Mota. Independent components of human brain morphology. *NeuroImage*, 226:117546, 2 2021. ISSN 1053-8119. doi: 10.1016/J.NEUROIMAGE.2020.117546.
- [9] Joel T. Nigg, Sarah L. Karalunas, Michael A. Mooney, Beth Wilmot, Molly A. Nikolas, Michelle M. Martel, Jessica Tipsord, Elizabeth K. Nousen, Colleen Schmitt, Peter Ryabinin, Erica D. Musser, Bonnie J. Nagel, and Damien A. Fair. The oregon adhd-1000: A new longitudinal data resource enriched for clinical cases and multiple levels of analysis. *Developmental*

cognitive neuroscience, 60, 4 2023. ISSN 1878-9307. doi: 10.1016/J.DCN.2023.101222. URL <https://pubmed.ncbi.nlm.nih.gov/36848718/>.

- [10] Marc M. Himmelberg, Ekin Tünçok, Jesse Gomez, Kalanit Grill-Spector, Marisa Carrasco, and Jonathan Winawer. Comparing retinotopic maps of children and adults reveals a late-stage change in how v1 samples the visual field. *Nature Communications* 2023 14:1, 14:1–15, 3 2023. ISSN 2041-1723. doi: 10.1038/s41467-023-37280-8. URL <https://www.nature.com/articles/s41467-023-37280-8>.
- [11] Michal Rafal Zareba, Magdalena Fafrowicz, Tadeusz Marek, Ewa Beldzik, Halszka Oginska, Anna Beres, Piotr Faba, Justyna Janik, Koryna Lewandowska, Monika Ostrogorska, Barbara Sikora-Wachowicz, Aleksandra Zyrkowska, and Aleksandra Domagalik. Neuroimaging of chronotype, sleep quality and daytime sleepiness: Structural t1-weighted magnetic resonance brain imaging data from 136 young adults. *Data in Brief*, 41:107956, 4 2022. ISSN 2352-3409. doi: 10.1016/J.DIB.2022.107956.
- [12] Allison C. Nugent, Adam G. Thomas, Margaret Mahoney, Alison Gibbons, Jarrod T. Smith, Antoinette J. Charles, Jacob S. Shaw, Jeffrey D. Stout, Anna M. Namyst, Arshitha Basavaraj, Eric Earl, Travis Riddle, Joseph Snow, Shruti Japee, Adriana J. Pavletic, Stephen Sinclair, Vinai Roopchansingh, Peter A. Bandettini, and Joyce Chung. The nimh intramural healthy volunteer dataset: A comprehensive meg, mri, and behavioral resource. *Scientific Data* 2022 9:1, 9:1–10, 8 2022. ISSN 2052-4463. doi: 10.1038/s41597-022-01623-9. URL <https://www.nature.com/articles/s41597-022-01623-9>.
- [13] David C. Van Essen, Stephen M. Smith, Deanna M. Barch, Timothy E.J. Behrens, Essa Yacoub, and Kamil Ugurbil. The wu-minn human connectome project: An overview. *NeuroImage*, 80:62–79, 10 2013. ISSN 1053-8119. doi: 10.1016/J.NEUROIMAGE.2013.05.041.
- [14] Kate Brody Nooner, Stanley J. Colcombe, Russell H. Tobe, Maarten Mennes, Melissa M. Benedict, Alexis L. Moreno, Laura J. Panek, Shaquanna Brown, Stephen T. Zavitz, Qingyang Li, Sharad Sikka, David Gutman, Saroja Bangaru, Rochelle Tziona Schlachter, Stephanie M. Kamiel, Ayesha R. Anwar, Caitlin M. Hinz, Michelle S. Kaplan, Anna B. Rachlin, Samantha

Adelsberg, Brian Cheung, Ranjit Khanuja, Chaogan Yan, Cameron C. Craddock, Vincent Calhoun, William Courtney, Margaret King, Dylan Wood, Christine L. Cox, A. M. Clare Kelly, Adriana Di Martino, Eva Petkova, Philip T. Reiss, Nancy Duan, Dawn Thomsen, Bharat Biswal, Barbara Coffey, Matthew J. Hoptman, Daniel C. Javitt, Nunzio Pomara, John J. Sidtis, Harold S. Koplewicz, Francisco Xavier Castellanos, Bennett L. Leventhal, and Michael P. Milham. The nki-rockland sample: A model for accelerating the pace of discovery science in psychiatry. *Frontiers in Neuroscience*, 6:32787, 10 2012. ISSN 1662453X. doi: 10.3389/FNINS.2012.00152/BIBTEX. URL www.frontiersin.org.

- [15] Meredith A Shafto, Lorraine K Tyler, Marie Dixon, Jason R Taylor, James B Rowe, Rhodri Cusack, Andrew J Calder, William D Marslen-Wilson, John Duncan, Tim Dalgleish, Richard N Henson, Carol Brayne, and Fiona E Matthews. The cambridge centre for ageing and neuroscience (cam-can) study protocol: a cross-sectional, lifespan, multidisciplinary examination of healthy cognitive ageing. *BMC neurology*, 14, 2014. ISSN 1471-2377. doi: 10.1186/S12883-014-0204-1. URL <https://pubmed.ncbi.nlm.nih.gov/25412575/>.
- [16] Jason R. Taylor, Nitin Williams, Rhodri Cusack, Tibor Auer, Meredith A. Shafto, Marie Dixon, Lorraine K. Tyler, Cam-CAN, and Richard N. Henson. The cambridge centre for ageing and neuroscience (cam-can) data repository: Structural and functional mri, meg, and cognitive data from a cross-sectional adult lifespan sample. *NeuroImage*, 144:262–269, 1 2017. ISSN 1095-9572. doi: 10.1016/J.NEUROIMAGE.2015.09.018. URL <https://pubmed.ncbi.nlm.nih.gov/26375206/>.
- [17] Pamela J. LaMontagne, Tammie LS. Benzinger, John C. Morris, Sarah Keefe, Russ Hornbeck, Chengjie Xiong, Elizabeth Grant, Jason Hassenstab, Krista Moulder, Andrei G. Vlassenko, Marcus E. Raichle, Carlos Cruchaga, and Daniel Marcus. Oasis-3: Longitudinal neuroimaging, clinical, and cognitive dataset for normal aging and alzheimer disease. *medRxiv*, page 2019.12.13.19014902, 12 2019. doi: 10.1101/2019.12.13.19014902. URL <https://www.medrxiv.org/content/10.1101/2019.12.13.19014902v1>.
- [18] Deanna J Greene, Jonathan M Koller, Jacqueline M Hampton, Victoria Wesevich, Andrew N

Van, Annie L Nguyen, Catherine R Hoyt, Lindsey McIntyre, Eric A Earl, Rachel L Klein, Joshua S Shimony, Steven E Petersen, Bradley L Schlaggar, Damien A Fair, and Nico U F Dosenbach. Behavioral interventions for reducing head motion during mri scans in children. *NeuroImage*, 171:234–245, 5 2018. ISSN 1095-9572. doi: 10.1016/J.NEUROIMAGE.2018.01.023. URL <https://pubmed.ncbi.nlm.nih.gov/29337280/>.

- [19] D P Hibar, L T Westlye, N T Doan, N Jahanshad, J W Cheung, C R K Ching, A Versace, A C Bilderbeck, A Uhlmann, B Mwangi, B Krämer, B Overs, C B Hartberg, C Abé, D Dima, D Grotegerd, E Sprooten, E Bøen, E Jimenez, F M Howells, G Delvecchio, H Temmingh, J Starke, J R C Almeida, J M Goikolea, J Houenou, L M Beard, L Rauer, L Abramovic, M Bonnin, M F Ponteduro, M Keil, M M Rive, N Yao, N Yalin, P Najt, P G Rosa, R Redlich, S Trost, S Hagenaars, S C Fears, S Alonso-Lana, T G M van Erp, T Nickson, T M Chaim-Avancini, T B Meier, T Elvsåshagen, U K Haukvik, W H Lee, A H Schene, A J Lloyd, A H Young, A Nugent, A M Dale, A Pfennig, A M McIntosh, B Lafer, B T Baune, C J Ekman, C A Zarate, C E Bearden, C Henry, C Simhandl, C McDonald, C Bourne, D J Stein, D H Wolf, D M Cannon, D C Glahn, D J Veltman, E Pomarol-Clotet, E Vieta, E J Canales-Rodriguez, F G Nery, F L S Duran, G F Busatto, G Roberts, G D Pearlson, G M Goodwin, H Kugel, H C Whalley, H G Ruhe, J C Soares, J M Fullerton, J K Rybakowski, J Savitz, K T Chaim, M Fatjó-Vilas, M G Soeiro-de Souza, M P Boks, M V Zanetti, M C G Otaduy, M S Schaufelberger, M Alda, M Ingvar, M L Phillips, M J Kempton, M Bauer, M Landén, N S Lawrence, N E M van Haren, N R Horn, N B Freimer, O Gruber, P R Schofield, P B Mitchell, R S Kahn, R Lenroot, R Machado-Vieira, R A Ophoff, S Sarró, S Frangou, T D Satterthwaite, T Hajek, U Dannlowski, U F Malt, V Arolt, W F Gattaz, W C Drevets, X Caseras, I Agartz, P M Thompson, and O A Andreassen. Cortical abnormalities in bipolar disorder: an mri analysis of 6503 individuals from the enigma bipolar disorder working group. *Molecular Psychiatry* 2018 23:4, 23:932–942, 5 2018. ISSN 1476-5578. doi: 10.1038/mp.2017.73. URL <https://www.nature.com/articles/mp201773>.

- [20] Peter N. Taylor, Yujiang Wang, Callum Simpson, Vytene Janiukstyte, Jonathan Horsley, Karoline Leiberger, Beth Little, Harry Clifford, Sophie Adler, Sjoerd Vos, Gavin Winston,

Andrew McEvoy, Anna Miserocchi, Jane de Tisi, and John Duncan. The imaging database for epilepsy and surgery (IDEAS). *arXiv*, 2024. doi: 10.48550/arXiv.2406.06731.

- [21] Christopher D Whelan, Andre Altmann, Juan A Botía, Neda Jahanshad, Derrek P Hibar, Julie Absil, Saud Alhusaini, Marina K M Alvim, Pia Auvinen, Emanuele Bartolini, Felipe P G Bergo, Tauana Bernardes, Karen Blackmon, Barbara Braga, Maria Eugenia Caligiuri, Anna Calvo, Sarah J Carr, Jian Chen, Shuai Chen, Andrea Cherubini, Philippe David, Martin Domin, Sonya Foley, Wendy França, Gerrit Haaker, Dmitry Isaev, Simon S Keller, Raviteja Kotikalapudi, Magdalena A Kowalczyk, Ruben Kuzniecky, Soenke Langner, Matteo Lenge, Kelly M Leyden, Min Liu, Richard Q Loi, Pascal Martin, Mario Mascalchi, Marcia E Morita, Jose C Pariente, Raul Rodríguez-Cruces, Christian Rummel, Taavi Saavalainen, Mira K Semmelroch, Mariasavina Severino, Rhys H Thomas, Manuela Tondelli, Domenico Tortora, Anna Elisabetta Vaudano, Lucy Vivash, Felix von Podewils, Jan Wagner, Bernd Weber, Yi Yao, Clarissa L Yasuda, Guohao Zhang, Nuria Bargalló, Benjamin Bender, Neda Bernasconi, Andrea Bernasconi, Boris C Bernhardt, Ingmar Blümcke, Chad Carlson, Gianpiero L Cavalleri, Fernando Cendes, Luis Concha, Norman Delanty, Chantal Depondt, Orrin Devinsky, Colin P Doherty, Niels K Focke, Antonio Gambardella, Renzo Guerrini, Khalid Hamandi, Graeme D Jackson, Reetta Kälviäinen, Peter Kochunov, Patrick Kwan, Angelo Labate, Carrie R McDonald, Stefano Meletti, Terence J O’Brien, Sebastien Ourselin, Mark P Richardson, Pasquale Striano, Thomas Thesen, Roland Wiest, Junsong Zhang, Annamaria Vezzani, Mina Ryten, Paul M Thompson, and Sanjay M Sisodiya. Structural brain abnormalities in the common epilepsies assessed in a worldwide enigma study. *Brain*, 141:391–408, 2 2018. ISSN 0006-8950. doi: 10.1093/BRAIN/AWX341.
- [22] Dorian Pustina, Brian Avants, Michael Sperling, Richard Gorniak, Xiaosong He, Gaele Doucet, Paul Barnett, Scott Mintzer, Ashwini Sharan, and Joseph Tracy. Predicting the laterality of temporal lobe epilepsy from pet, mri, and dti: A multimodal study. *NeuroImage: Clinical*, 9:20–31, 2015. ISSN 2213-1582. doi: <https://doi.org/10.1016/j.nicl.2015.07.010>. URL <https://www.sciencedirect.com/science/article/pii/S2213158215001291>.

- [23] W Evan Johnson, Cheng Li, and Ariel Rabinovic. Adjusting batch effects in microarray expression data using empirical Bayes methods. *Biostatistics*, 8(1):118–127, 2007. doi: 10.1093/biostatistics/kxj037. URL <http://biostatistics.oxfordjournals.org/>.
- [24] Yu-Chi Chen, Aurina Arnatkevičiūtė, Eugene McTavish, James C Pang, Sidhant Chopra, Chao Suo, Alex Fornito, and Kevin M Aquino. The individuality of shape asymmetries of the human cerebral cortex. *eLife*, 11:e75056, oct 2022. ISSN 2050-084X. doi: 10.7554/eLife.75056. URL <https://doi.org/10.7554/eLife.75056>.
- [25] Yujiang Wang, Karoline Leiberger, Nathan Kindred, Christopher R Madan, Colline Poirier, Christopher I Petkov, Peter N Taylor, and Bruno CC Mota. Neuro-evolutionary evidence for a universal fractal primate brain shape. *eLife*, 2023. doi: 10.7554/eLife.92080.2.
- [26] Karoline Leiberger, Timo Blattner, Bethany Little, Victor B. B. Mello, Fernanda H. P. de Moraes, Christian Rummel, Peter N. Taylor, Bruno Mota, and Yujiang Wang. Multi-scale cortical morphometry reveals pronounced regional and scale-dependent variations across the lifespan. *arXiv*, 11 2023. doi: 10.48550/arXiv.2311.13501.
- [27] Barbora Reháková Bučková, Charlotte Fraza, Rastislav Reháková, Marián Kolenič, Christian Beckmann, Filip Španiel, Andre Marquand, and Jaroslav Hlinka. Using normative models pre-trained on cross-sectional data to evaluate longitudinal changes in neuroimaging data. *bioRxiv*, pages 2023–06, 2023.
- [28] Bruce Fischl. Freesurfer. *NeuroImage*, 62:774–781, 8 2012. ISSN 1053-8119. doi: 10.1016/J.NEUROIMAGE.2012.01.021.
- [29] Marie Schaer, Meritxell Bach Cuadra, Nick Schmansky, Bruce Fischl, Jean Philippe Thiran, and Stephan Eliez. How to measure cortical folding from mr images: a step-by-step tutorial to compute local gyrification index. *Journal of visualized experiments : JoVE*, pages 1–8, 2012. ISSN 1940-087X. doi: 10.3791/3417. URL <https://pubmed.ncbi.nlm.nih.gov/22230945/>.
- [30] Rahul S. Desikan, Florent Ségonne, Bruce Fischl, Brian T. Quinn, Bradford C. Dickerson, Deborah Blacker, Randy L. Buckner, Anders M. Dale, R. Paul Maguire, Bradley T. Hyman,

- Marilyn S. Albert, and Ronald J. Killiany. An automated labeling system for subdividing the human cerebral cortex on mri scans into gyral based regions of interest. *NeuroImage*, 31: 968–980, 7 2006. ISSN 1053-8119. doi: 10.1016/J.NEUROIMAGE.2006.01.021.
- [31] Yujiang Wang, Joe Nocus, Marcus Kaiser, and Bruno Mota. Universality in human cortical folding in health and disease. *Proceedings of the National Academy of Sciences of the United States of America*, 113:12820–12825, 11 2016. ISSN 10916490. doi: 10.1073/PNAS.1610175113. URL <https://www.pnas.org/doi/abs/10.1073/pnas.1610175113>.
- [32] Bruno Mota and Suzana Herculano-Houzel. Cortical folding scales universally with surface area and thickness, not number of neurons. *Science*, 349:74–77, 2015. ISSN 10959203. doi: 10.1126/science.aaa9101.
- [33] Yujiang Wang, Joe Nocus, Luis Peraza Rodriguez, Peter Neal Taylor, and Bruno Mota. Human cortical folding across regions within individual brains follows universal scaling law. *Communications Biology* 2019 2:1, 2:1–8, 5 2019. ISSN 2399-3642. doi: 10.1038/s42003-019-0421-7. URL <https://www.nature.com/articles/s42003-019-0421-7>.
- [34] Karoline Leiberg, Christoforos Papasavvas, and Yujiang Wang. Local morphological measures confirm that folding within small partitions of the human cortex follows universal scaling law. *Lecture Notes in Computer Science (including subseries Lecture Notes in Artificial Intelligence and Lecture Notes in Bioinformatics)*, 12907 LNCS:691–700, 2021. ISSN 16113349. doi: 10.1007/978-3-030-87234-2_65/. URL https://link.springer.com/chapter/10.1007/978-3-030-87234-2_65.
- [35] Fiona Elizabeth Smith, Peter Edward Thelwall, Joe Nocus, Carly Jay Flowers, Andrew Matthew Blamire, and David Andrew Cousins. 3d 7li magnetic resonance imaging of brain lithium distribution in bipolar disorder. *Molecular Psychiatry*, 23:2184–2191, 2018. ISSN 14765578. doi: 10.1038/s41380-018-0016-6.

Acknowledgements:

We thank members of the Computational Neurology, Neuroscience & Psychiatry Lab (www.cnnplab.com) for discussions on the analysis and manuscript. The full list of acknowledgements for the normative data is provided in the supplementary materials. We thank all participants who generously contributed their time and data.

Funding

BL, YW, and KL were supported by the EPSRC (EP/Y016009/1). YW and PT were supported by UKRI Future Leaders Fellowships (MR/V026569/1, MR/T04294X/1). The Bipolar Lithium Imaging and Spectroscopy Study (BLISS) project was funded by the Medical Research Council (Clinician Scientist Fellowship BH135495 to DAC). The normative MEG UK data collection was supported by an MRC UK MEG Partnership Grant, MR/K005464/1. GPW and the collection of control data for the UCLH dataset were supported by the MRC (G0802012 and MR/M00841X/1).

The funders did not have a role in study conception, design, data collection, data analysis, interpretation of the data, preparation of the article, or article submission.

Author contributions

Conceptualization: BL, KL, and YW. Methodology: BL, KL, and YW. Investigation: BL, NA, AS, KL, and YW. Visualization: BL, KL, PT, and YW. Funding acquisition: GPW, JSD, DAC, PT, and YW. Project administration: BL and YW. Supervision: YW. Writing – original draft: BL. Writing – review & editing: BL, NA, AS, GPW, JSD, DAC, PT, KL, and YW.

Competing interests

There are no competing interests to disclose.

Data and materials availability

Normative data may be available at the discretion of the data holders, please see the website of individual datasets for more information. The subset of the IDEAS mesial TLE dataset is freely available with the associated paper (20).

List of supplementary materials:

- Normative Data
 - Table S1.1
- Statistical Modelling
 - Table S2.1
 - Fig. S2.1 to S2.5
- Additional Acknowledgements

Supplementary Materials:

S1 Normative data

Dataset (site)	Sample size [n]	Age in years [median(range)]	Sex [n female (%)]	Location [Country]	FreeSurfer [Version]
ADHD1000	153	11 (7 - 21)	79 (51.6%)	USA	7.3.2
BLISS	26	49 (20 - 64)	12 (46.2%)	UK	6.0.1
CamCAN (s1)	495	50 (19 - 89)	259 (52.3%)	UK	5.3.0
CamCAN (s2)	83	59 (19 - 86)	49 (59.0%)	UK	5.3.0
Chronotype	126	24 (18 - 35)	82 (65.1%)	Poland	7.3.2
Greene-HM	22	11 (6 - 16)	9 (40.9%)	USA	7.3.2
HCP	678	29 (22 - 37)	370 (54.6%)	USA	5.2
MEGUK (Aston1)	29	23 (18 - 49)	25 (86.2%)	UK	7.3.2
MEGUK (Aston2)	69	33 (18 - 63)	39 (56.5%)	UK	7.3.2
MEGUK (Cambridge)	71	42 (19 - 80)	37 (52.1%)	UK	7.3.2
MEGUK (Glasgow)	24	26 (18 - 34)	13 (54.2%)	UK	7.3.2
MEGUK (Oxford)	63	40 (20 - 80)	34 (54.0%)	UK	7.3.2
NCL-dementia (s1)	29	77 (62 - 85)	11 (37.9%)	UK	6.0.1
NCL-dementia (s2)	26	74 (61 - 87)	14 (53.8%)	UK	6.0.1
NIMH-IHV (s1)	48	27 (18 - 63)	35 (72.9%)	USA	7.3.2
NIMH-IHV (s2)	54	33 (21 - 71)	48 (88.9%)	USA	7.3.2
NKI	790	39 (6 - 85)	489 (61.9%)	USA	6.0.1
OASIS3	355	67 (42 - 95)	228 (64.2%)	USA	7.3.2
Stanford-CR	40	22 (5 - 27)	19 (47.5%)	USA	7.3.2
UCLH (s1)	28	37 (19 - 64)	16 (57.1%)	UK	7.3.2
UCLH (s3)	67	39 (19 - 65)	43 (64.2%)	UK	7.3.2
Total	3,276	33 (5 - 95)	1,911 (58.3%)		

Table S1.1: Descriptive statistics of each study dataset included in the normative model.

S2 Statistical modelling

Model formula

For the normative model, we assume the morphological data, measured in all metrics including cortical thickness, volume, surface area, tension K , shape S , and isometric size I , follow a flexible sinh-arcsinh (shash) distribution, which allows for non-normal modelling of the data in which the first four moments of the distribution can vary as functions of explanatory variables. All metrics are transformed to a logscale before statistical modelling. We use `gamlss` (<https://www.rdocumentation.org/packages/gamlss/versions/5.4-12/topics/gamlss>) to simultaneously model the parameters (first four moments) of the distribution as response variables of the explanatory variables `sex`, `age`, and `scanning site`. We use the model formulae:

$$\mu \sim 1 + \text{sex} + s(\text{age}) + (1|\text{site})$$

$$\sigma \sim 1 + \text{sex} + s(\text{age}) + (1|\text{site})$$

$$\nu \sim 1 + \text{sex} + s(\text{age})$$

$$\tau \sim 1 + s(\text{age})$$

- The mean (μ) depends on `sex` (fixed effect), `site` (random effect), and a smooth function of `age`.
- The standard deviation (σ) depends on the `site` (random effect) and a smooth function of `age`.
- The skew (ν) depends on a smooth function of `age`.
- The kurtosis (τ) depends on a smooth function of `age`.

We fitted this model to the normative datasets ($n \sim 3500$) for each metric and cortical region independently.

To test our model formula, we fitted alternative models to our data, changing one model term at a time. This resulted in the comparison of 11 models in total. The model as described above

is considered the default (Model 1 in figures S2.1, S2.2, S2.3). In models 2-11, the formulae of all parameters were kept the same as in model 1, except as described below:

$$\text{Model 2: } \mu \sim 1 + s(\text{age}) + (1|\text{site})$$

$$\text{Model 3: } \sigma \sim 1 + s(\text{age}) + (1|\text{site})$$

$$\text{Model 4: } \nu \sim 1 + s(\text{age})$$

$$\text{Model 5: } \tau \sim 1 + \text{sex} + s(\text{age})$$

$$\text{Model 6: } \nu \sim 1 + \text{sex} + s(\text{age}) + (1|\text{site})$$

$$\text{Model 7: } \tau \sim 1 + s(\text{age}) + (1|\text{site})$$

$$\text{Model 8: } \mu \sim 1 + \text{sex} + \text{age} + (1|\text{site})$$

$$\text{Model 9: } \sigma \sim 1 + \text{sex} + \text{age} + (1|\text{site})$$

$$\text{Model 10: } \nu \sim 1 + \text{sex} + \text{age}$$

$$\text{Model 11: } \tau \sim 1 + \text{age}$$

I.e., models 2-5 removed/introduced a sex term to the four parameters, models 6-7 introduced a site effect to the skew and kurtosis, and models 8-11 simplified the smooth function of age to a linear term in all four parameters. We computed AICs (Akaike information criterion) for each model fit in each metric and cortical region, and assessed the optimal model for each metric and region by computing weighted relative AICs (figures S2.1, S2.2, S2.3).

Generally, our model fitted the data better or similarly well as the alternative models. In a subset of cortical regions, model 6 with a random site effect on the skew had a significantly better fit. However, we opted not to include this term in our final model for two reasons: a), to keep the model formula consistent across metrics and regions for comparability, and b) to allow us to apply the normative model to new datasets with small healthy control samples, which would make an accurate estimation of site-specific skew impossible.

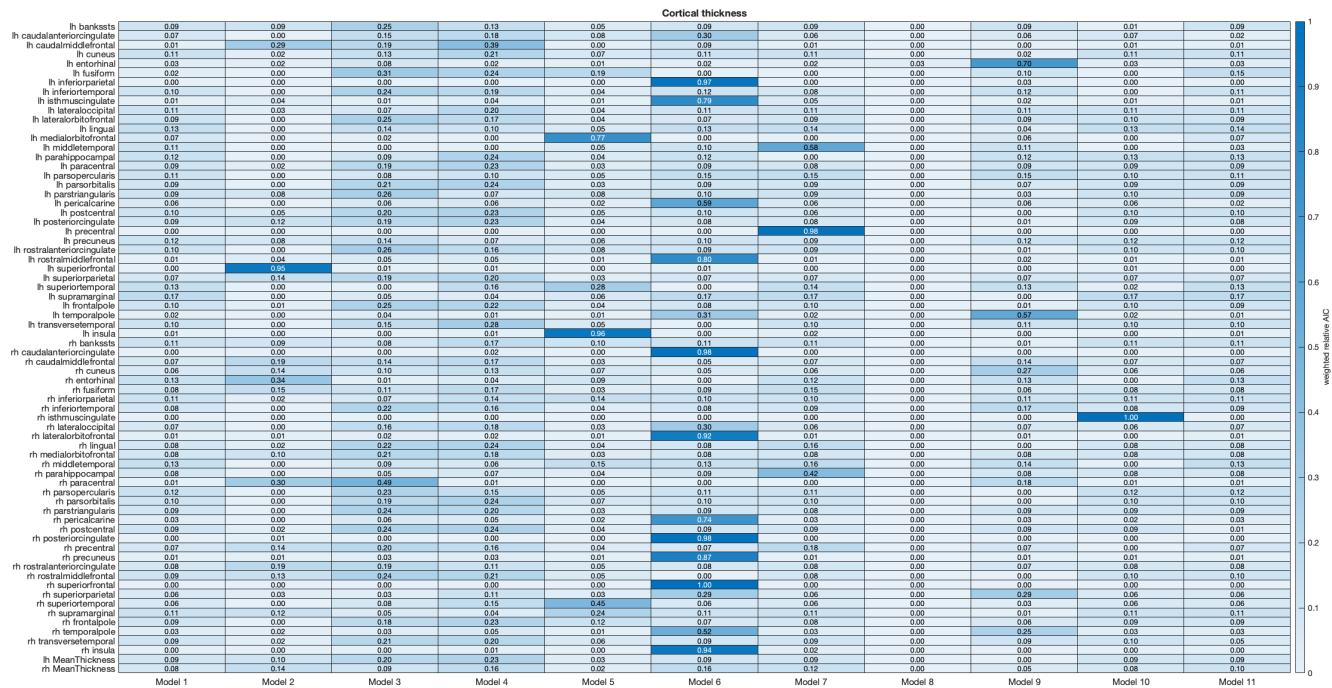
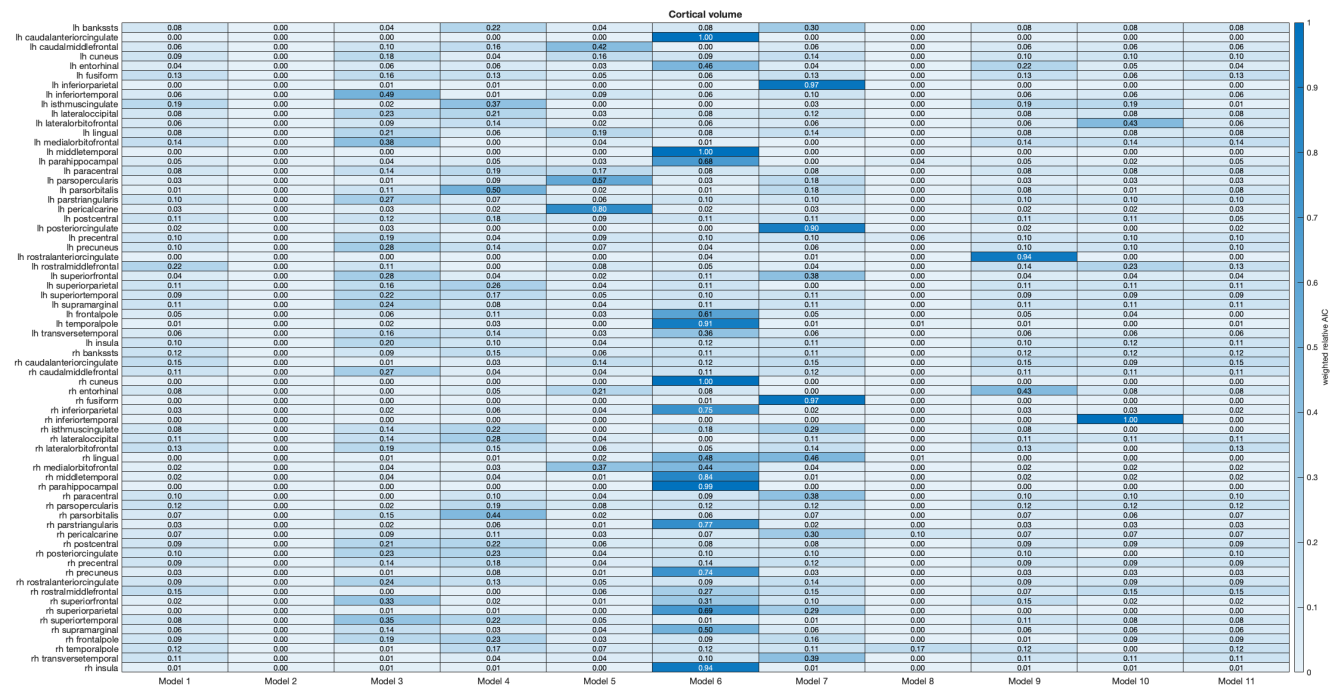


Fig. S2.1: Weighted relative AIC of 11 gamlss models fitted for cortical thickness. Darker colour indicates higher probability that the model is optimal for that metric and region out of the 11 models tested. Rows correspond to 68 regions (Desikan-Killiany atlas) as well as left and right hemisphere mean thickness. Columns correspond to 11 model formulae.



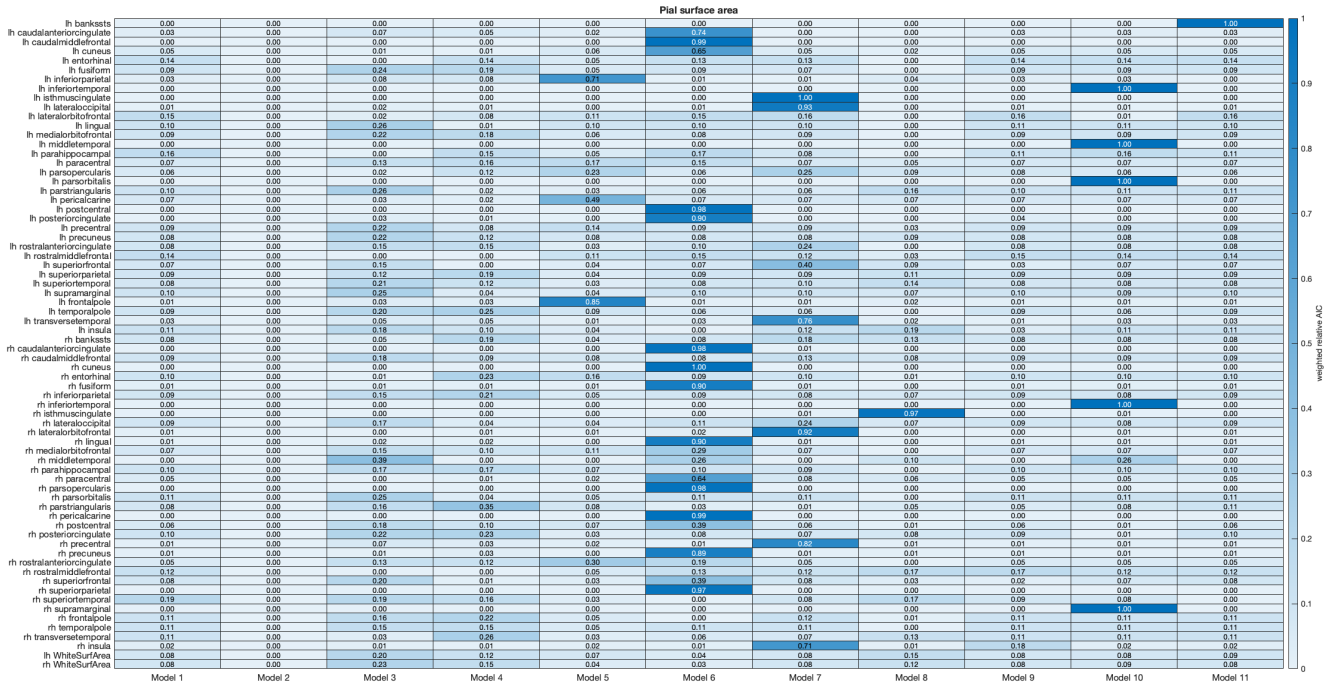


Fig. S2.3: Weighted relative AIC of 11 gamlss models fitted for pial surface area. Darker colour indicates higher probability that the model is optimal for that metric and region out of the 11 models tested. Rows correspond to 68 regions (Desikan-Killiany atlas) as well as left and right hemisphere total surface area. Columns correspond to 11 model formulae.

Application to new data

To apply the model to new datasets, we fitted it to the new data assuming it was from one of the scanning sites used for training, to predict model parameters and calculate residuals. This removed site and sex effects from the data. Site-specific mean and variance were then estimated as the mean and variance of the residuals of the new site’s healthy controls. The exact steps of this algorithm are described in table S2.4.

Here, steps 5-7 are similar to steps 2-4, but remove the standard deviation from the data rather than the mean. Whilst the mean of a dataset can be estimated reasonably reliably even from small samples, the estimation of standard deviation requires a larger sample. For this reason, we use even small (>10 subjects) healthy control data to estimate the new site’s mean (step 3), but require at least 30 subjects for the estimation of the new site’s standard deviation (step 6).

To compute centiles, we estimate $\mu'_{hc} = \text{mean}(y_3)$ again from the healthy controls. We then use that site mean, the site standard deviation (σ_{hc}), and the skew and kurtosis from the normative

model (ν_{nm} and τ_{nm}) to get quantiles for each subject and calculate their centiles (Figure S2.5).

Step	Change	Explanation
1	Predict $\mu_{nm}, \sigma_{nm}, \nu_{nm}, \tau_{nm}$ for each subject from normative model.	Predict distribution parameters for each new subject based on their age and sex, but with their site set to one of the normative sites (site A).
2	$y_1 = y - \mu_{nm}$	Calculate residuals for each subject relative to site A by subtracting the predicted μ , which removes age and sex effects and centres the new site around the mean of site A.
3	Estimate $\mu_{hc} = \text{mean}(y_1)$ from healthy controls.	Estimate the mean of the residuals from the healthy controls. This is the site-specific offset of the new site relative to site A.
4	$y_2 = y_1 - \mu_{hc}$	Calculate residuals for each subject relative to their site mean.
5	$y_3 = y_2 / \sigma_{nm}$	Divide by the standard deviation predicted by the normative model, to z-score subjects relative to the variance in site A.
6	Estimate $\sigma_{hc} = \text{std}(y_3)$ from healthy controls or $\sigma_{hc} = \text{mean}(\sigma_{sites})$	If the new site has more than 30 controls, estimate the standard deviation from the controls relative to site A. or If there are fewer than 30 controls, compute the mean of the site-specific standard deviations across normative sites (obtained as their σ coefficients) as an estimate standard deviation instead.
7	$zscore = y_3 / \sigma_{hc}$	The data is z-scored by dividing by the site-specific standard deviation.

Table S2.1: Steps to apply the normative model to new data from an unseen scanning site. Here, y is the measured data of one subject in a single cortical region in one metric (e.g. thickness). y_n refers to the data after successive steps of manipulation. $\mu_{nm}, \sigma_{nm}, \nu_{nm}, \tau_{nm}$ are the mean, standard deviation, skew and kurtosis predicted for one subject by the normative model. μ_{hc} and σ_{hc} are the site-specific mean and standard deviation relative to a normative site A.

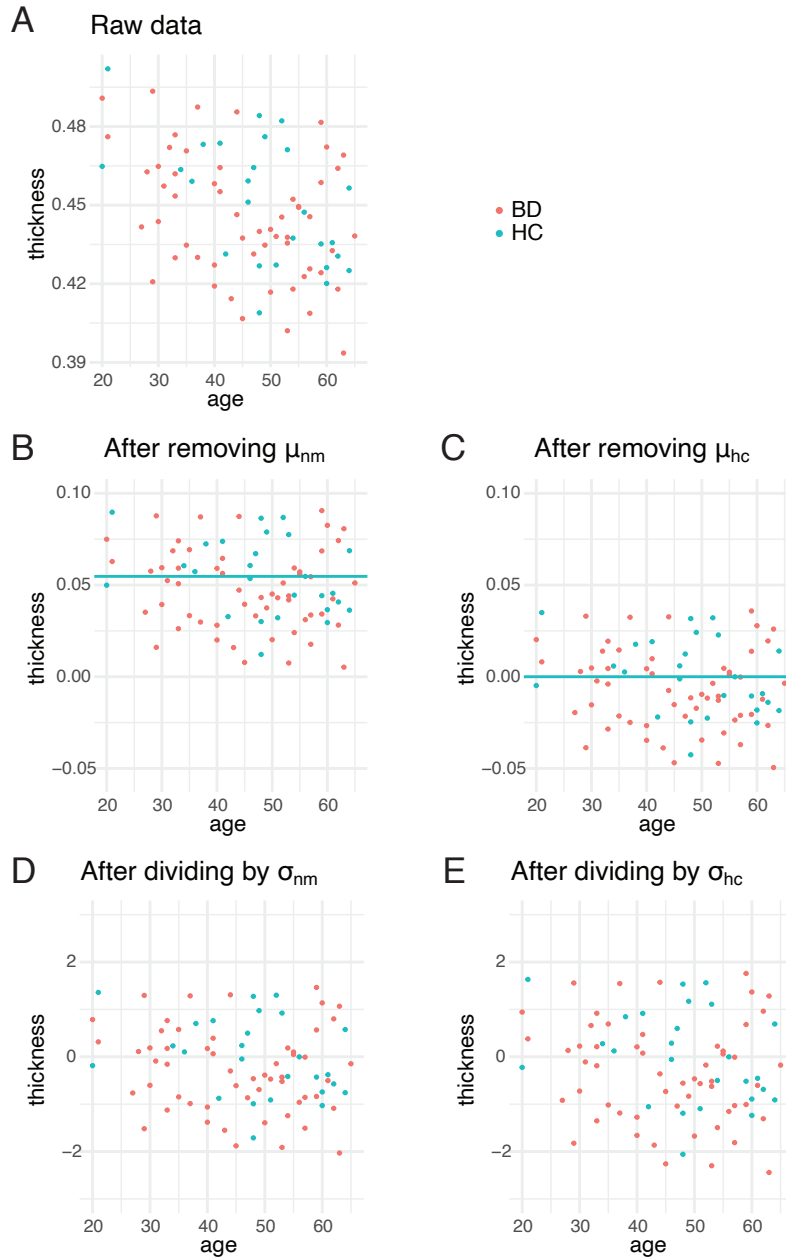


Fig. S2.4: Application of normative model to unseen data. Plots show cortical thickness for one example region. **A** Raw data from new scanning site. **B** Data after removing the mean μ_{nm} estimated from the normative model (step 2.). The blue line indicates the healthy control mean μ_{hc} . **C** Data after removing the site-specific mean μ_{hc} (step 4.). **D** Data after dividing by the standard deviation σ_{nm} estimated from the normative model (step 5.). **E** Data after dividing by the site-specific standard deviation σ_{hc} (step 7.).

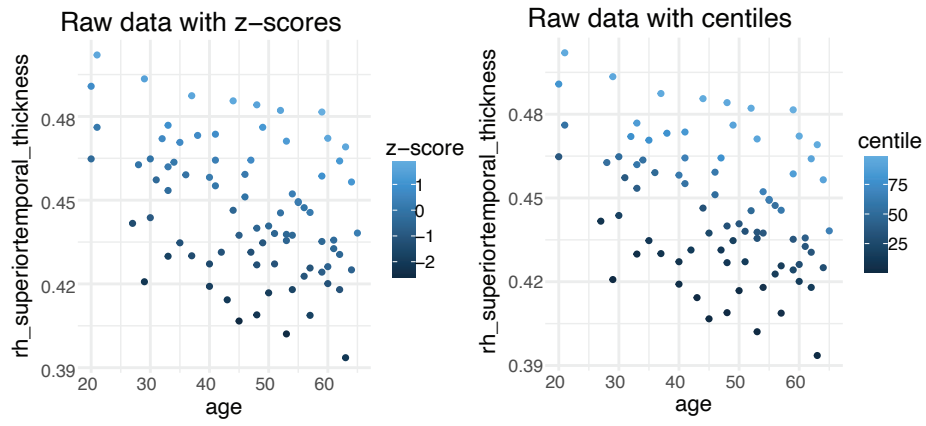


Fig. S2.5: Z-scores and centiles of unseen data.

S3 Additional Acknowledgements

Cambridge Centre for Ageing and Neuroscience (CamCAN). CamCAN funding was provided by the UK Biotechnology and Biological Sciences Research Council (grant number BB/H008217/1), together with support from the UK Medical Research Council and the University of Cambridge, UK.

OASIS-3 provided data: Longitudinal Multimodal Neuroimaging: Principal Investigators: T. Benzinger, D. Marcus, J. Morris; NIH P30 AG066444, P50 AG00561, P30 NS09857781, P01 AG026276, P01 AG003991, R01 AG043434, UL1 TR000448, R01 EB009352. AV-45 doses were provided by Avid Radiopharmaceuticals, a wholly-owned subsidiary of Eli Lilly. HCP data were provided in part by the Human Connectome Project, WU-Minn Consortium (Principal Investigators: David Van Essen and Kamil Ugurbil; 1U54MH091657) funded by the 16 NIH Institutes and Centers that support the NIH Blueprint for Neuroscience Research; and by the McDonnell Center for Systems Neuroscience at Washington University.

The Oregon ADHD1000 raw data is publicly available on the NIMH Data Archive (NDA) under #1938.

We thank the NIMH Office of the Clinical Director, the outpatient behavioral health clinic and NMR center for providing support for the data collection. This work utilized the computational resources of the NIH HPC Biowulf cluster <http://hpc.nih.gov>.

We thank Anna Beres, Koryna Lewandowska, Monika Ostrogorska, Barbara Sikora-Wachowicz, Aleksandra Zyrkowska, Justyna Janik, Kamil Cepuch, and Piotr Faba for assistance with participant recruitment and data collection of chronotype dataset. They are funded by Polish National Science Centre (NCN) Grant 2013/08/M/HS6/00042 and Grant 2013/08/W/NZ3/00700.

Greene data collection was supported by National Institutes of Health Grants K01MH104592 (DJG), K23NS088590, UL1TR000448 (NUFD), R01MH096773, R00MH091238, UL1TR000128, MH110766, U01DA041148 (DAF), P30NS098577 (to the Neuroimaging Informatics and Analysis Center), and U54HD087011 (to the Eunice Kennedy Shriver National Institute Of Child Health & Human Development of the National Institutes of Health to the Intellectual and Developmental Disabilities Research Center at Washington University; BLS), the Tourette Association of America

(DJG), the McDonnell Center for Systems Neuroscience, the Mallinckrodt Institute of Radiology (DJG, NUFD), the DeStefano Family Foundation (DAF), the Jacobs Foundation, and the Child Neurology Foundation (NUFD).